

Theory of Seamless-Scanning Periodic Leaky-Wave Antennas based on \mathcal{PT} -Symmetry with Time to Space Mapping

Amar Al-Bassam, *Member, IEEE*, Simon Otto, *Member, IEEE*, Dirk Heberling, *Senior Member, IEEE*,
and Christophe Caloz, *Fellow, IEEE*

Abstract—Periodic Leaky-Wave Antennas (P-LWA) offer highly directive and space-scanning radiation. Unfortunately, they have been plagued by the “broadside issue”, characterized by a degradation in gain when the antenna’s main beam is steered across broadside. While this issue has been addressed by circuit and network approaches, a related fundamental and general electromagnetic theory has been lacking. This paper fills this gap. We first show that a P-LWA is a \mathcal{PT} -symmetric system, whose even- and odd-mode coupling in the complex space of temporal frequencies leads to the characteristic pair of two-sheet Riemann surfaces. We observe that the branch cuts of these surfaces, which form the well-known \mathcal{PT} -symmetric double pitchfork spectrum, correspond to the “balanced frequency” condition, while the branch point at the junction of the pitchforks, is an exceptional point that corresponds to the “ Q -balanced” condition, two conditions that were previously shown to be the conditions for eliminating the broadside issue. In order to acquire an independent and rigorous interpretation of this spectrum, we further transform the coupled complex temporal eigenfrequencies into complex spatial eigenfrequencies. We identify the resulting spatial frequencies as coupled forward-backward modes, with frequency-independent imaginary parts (leakage factors), a condition for P-LWA equalization across broadside. Finally, we derive the scattering parameters of the P-LWA and show that matching is achieved only at one of the two ends of the P-LWA structure. This work both provides a solid foundation to the theory of P-LWAs and represents an original contribution to the field of \mathcal{PT} -symmetry.

Index Terms—Leaky-wave antennas, periodic structures, space scanning, complex temporal and spatial frequencies, space-time mapping, coupled-mode theory, \mathcal{PT} -symmetry, exceptional point.

I. LIST OF SYMBOLS

TIME ANALYSIS (RESONATOR PROBLEM)

$x_{e,o}$	even- (or symmetric-) mode or odd- (or antisymmetric-) mode eigenquantity x
$\psi_{t;e,o}$	complex temporal eigenfrequency electromagnetic field: $\psi_{t;e,o}(t, z) = \exp(j\xi_{e,o}t)f_{e,o}(\beta z)$,
ξ	complex temporal eigenfrequency: $\xi = \omega + j\zeta$
ω	real part of ξ , i.e., usual (angular) frequency
ζ	imaginary part of ξ , i.e., inverse of the relaxation time
Q	quality factor: $Q = \omega/(2\zeta)$
Φ	periodic boundary condition (PBC) phase shift, i.e., phase shift between the two terminals of the unit cell
$x_{t;1,2}$	coupled-mode (coupling between the even and odd eigenmodes) temporal eigenquantity x_t number 1 or 2
$\psi_{t;1,2}$	coupled-mode electromagnetic field: $\psi_{t;1,2}(t, z) = \exp(j\xi_{1,2}t)f_{1,2}(\beta z)$, where $f_{1,2}(\cdot) = a_{1,2} \cos(\cdot) + b_{1,2} \sin(\cdot)$
κ_t	temporal coupling factor between even and odd modes
$\kappa_{t,ga}$	temporal coupling factor due to geometrical asymmetry
κ_{EP}	temporal coupling factor at the exceptional point

SPACE ANALYSIS (WAVEGUIDE PROBLEM)

x_{\pm}	forward (+) and backward (−) space harmonic (SH)
$\psi_{s,\pm}$	complex spatial eigenfrequency electromagnetic field: $\psi_{s,\pm}(z, t) = \exp(-\gamma_{\pm}z) \exp(j\omega t)$
γ	complex spatial frequency, or wavenumber: $\gamma = \alpha + j\beta$
α	real part of γ , or attenuation constant
β	imaginary part of γ , or phase constant
$x_{s;1,2}$	coupled-mode (between the forward and backward SHs) eigenquantity x_s number 1 or 2
$\psi_{s;1,2}$	spatial coupled-mode electromagnetic field: $\psi_{s;1,2}(t, z) = \exp(-\gamma_{1,2}z) \exp(j\omega t)$
κ_s	spatial coupling factor between the forward and backward SHs
$\kappa_{s,ga}$	spatial coupling factor due to geometric asymmetry
θ_{mb}	radiation angle of the main beam of the P-LWA: $\theta_{mb} \approx \sin^{-1}(\beta/k_0)$, where k_0 is the free-space wavenumber, $k_0 = \omega/c$, with c being the speed of light in free-space

II. INTRODUCTION

Leaky-wave antennas are traveling-wave structures that support faster-than-light waves, enabling electromagnetic radiation with frequency scanning [1]–[3]. These antennas can be uniform or periodic; however, the former are limited to

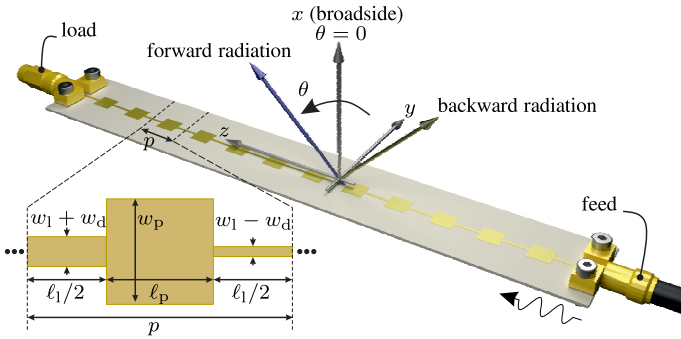


Fig. 1. Structure and operation of a Periodic Leaky-Wave Antenna (P-LWA), illustrated through the specific case of a Series-Fed Patch (SFP) design. This SFP-P-LWA [9] will be used as a representative example throughout the paper; however, the proposed theory is applicable to any P-LWA. The geometrical parameters $l_1 = 3.5$ mm, $l_p = 3.05$ mm, $w_1 = 0.3$ mm and $w_p = 3.3$ mm with a substrate height of 508 μm and $\epsilon_r = 3.66$ are kept constant throughout the paper, while the parameter w_d is varied, with $w_d = 0$ and $w_d \neq 0$ representing a symmetric and an asymmetric structure, respectively, with respect to the transverse (y) direction.

radiating within a partial sector of space [4], while the latter provide full-space scanning capability [3]. Therefore, this paper will focus on Periodic Leaky-Wave Antennas (P-LWAs), illustrated by the example in Fig. 1. Being non-resonant, such antennas can be electrically very long, providing significant directivity, without requiring a complex feeding network as antenna arrays. Consequently, they find applications in many areas, including communication [5], real-time spectral analysis [6], sensing [7] and imaging [8].

Since their inception over eighty years ago [10], P-LWAs have been plagued by the so-called “broadside issue” [1], [2], characterized by a degradation in gain when the antenna’s main beam is steered across broadside ($\theta = 0$ in Fig. 1). This phenomenon occurs due to the phase matching of forward and backward space-harmonics, resulting in a standing wave regime that creates an “open stop-band” [1],¹ reflecting most of this incident energy back to the source. The broadside issue was addressed in recent years, using a transmission-line network matching approach [11] and a circuit modeling approach [12]–[15], both revealing the necessity of structural *asymmetry*. Figure 2 presents typical radiation patterns for a P-LWA, with Fig. 2(a) showing the broadside gain degradation for a symmetric structure (the broadside issue)² and Fig. 2(b) showing the broadside gain equalization for a structure with optimal asymmetry (resolution of the broadside issue). However, a *comprehensive theory* rigorously explaining these symmetry-related phenomena has remained elusive to date.

Here, we address this gap by presenting the first complete and rigorous electromagnetic theory of the broadside issue, and, by extension, of P-LWAs in general, using the powerful concept of parity-time symmetry, or \mathcal{PT} -symmetry [16],

¹The term “open” in “open stopband” refers to the fact that the stopband occurs in an open (radiative) system rather than in a closed (wave-guided) one.

²The level of gain degradation at broadside varies among structures. Specifically, the structure in the example of Fig. 1 still considerably radiates at broadside, about 6 dB below the off-broadside gain (Fig. 2), due to relatively large transverse (x -direction) radiative metallic parts (here patches).

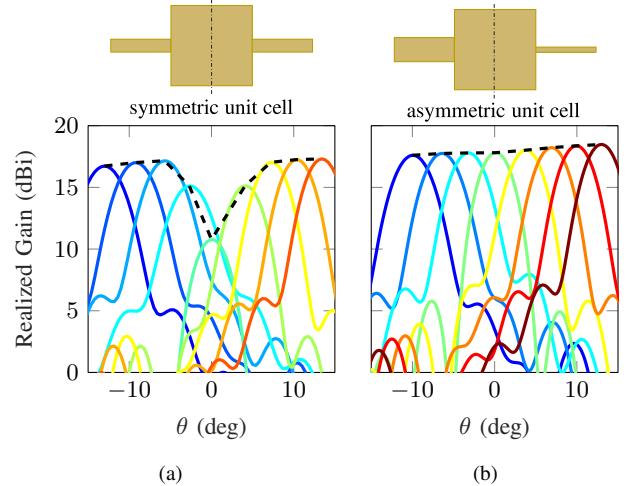


Fig. 2. Broadside radiation patterns at different frequencies around broadside for the SFP-P-LWA in Fig. 1 with (a) a symmetric unit cell and (b) an optimally asymmetric unit cell.

[17]. Specifically, we demonstrate that a P-LWA is a \mathcal{PT} -symmetric system with an Exceptional Point (EP), and show that operating the antenna at this EP is the key to achieving equalized gain across broadside or, equivalently, seamless full-space scanning.

The paper is organized as follows. Following the list of symbols in Sec. I and this introduction, Sec. II, Sec. III recalls the fundamentals of \mathcal{PT} -symmetry, including the underpinning notion of gain-loss systems, the mathematical formulation of \mathcal{PT} -symmetry in terms of commutation, the related complex eigenspectra and their EP. Then, Sec. IV conducts a time-domain analysis of the P-LWA system that determines its coupled-mode complex eigenfrequencies, plots the corresponding Riemann surfaces and points out the related \mathcal{PT} -symmetry, identifies its EP in the frequency balanced regime, and shows that this EP corresponds to the Q -balancing condition described in [14]. Next, Sec. V maps these complex temporal eigenfrequencies to their spatial counterparts, demonstrating that the EP corresponds to the real part of the spatial eigenfrequency (or leakage factor) being independent of frequency, a condition that enables uniform scanning through broadside. Finally, Sec. VI performs a space analysis that determines the related coupled complex eigenfrequencies and derives the scattering coefficients in the forward and backward directions, revealing that one direction is matched while the other is not. Concluding remarks are presented in Sec. VII.

III. \mathcal{PT} -SYMMETRY AND EXCEPTIONAL POINTS

\mathcal{PT} -symmetry is a concept that originates in quantum mechanics [16], but that also applies to classical optics [18]–[23]. A system is said to be \mathcal{PT} -symmetric if its non-Hermitian and yet has real eigenvalues. Such a situation occurs in *coupled gain-loss systems* [17], [22], such as the system shown in Fig. 3(a), featuring two interconnected box resonators—with gain and the other with loss—linked by a coupling duct. This system exhibits \mathcal{PT} -symmetry because its evolution is

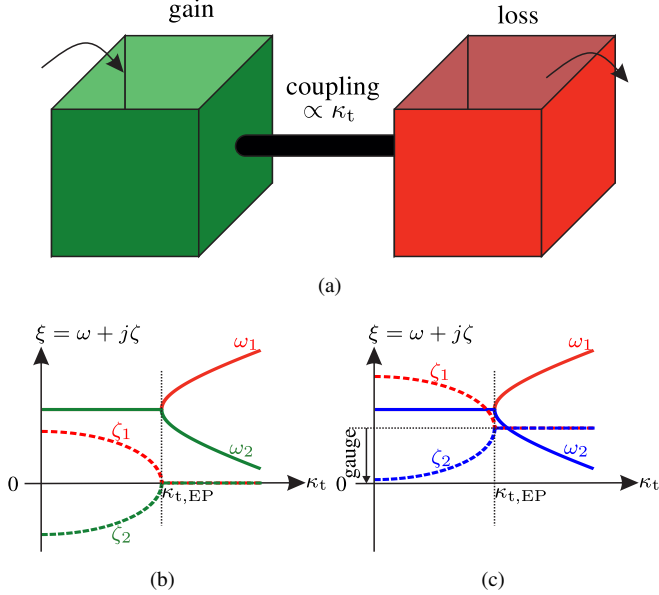


Fig. 3. \mathcal{PT} -symmetric system, composed of a gain box (box into which energy is added) and a loss box (box from which energy is removed), coupled by a duct (adapted from [17]). (a) Coupled-resonator system. (b) Complex eigenfrequencies of the system in (a) versus its coupling coefficient, κ_t . (c) Complex eigenfrequencies of the gauge-transformed loss-loss version of the system in (a).

identical if i) it is successively subjected to a \mathcal{T} or time reversal operations ($t \rightarrow -t$), equivalent to swapping gain and loss, and a \mathcal{P} or space reversal operation ($x \rightarrow -x$), equivalent to exchanging the two boxes, and ii) if the time reversal and space reversal operations are performed in the opposite order.

Mathematically, the \mathcal{PT} -symmetry of a system described by the Hamiltonian \mathcal{H} may be formulated as [17]

$$\begin{aligned}
 (\mathcal{PT})\mathcal{H}(\mathcal{PT})^{-1} &= (\mathcal{PT})\mathcal{H}(\mathcal{T}^{-1}\mathcal{P}^{-1}) \\
 &= \mathcal{P}(\mathcal{T}\mathcal{H}\mathcal{T}^{-1})\mathcal{P}^{-1} \\
 &= \mathcal{P}\mathcal{H}^*\mathcal{P} \\
 &= \mathcal{H},
 \end{aligned} \tag{1a}$$

or, equivalently, by the commutation

$$[\mathcal{PT}, \mathcal{H}] = (\mathcal{PT})\mathcal{H} - \mathcal{H}(\mathcal{PT}) = 0. \tag{1b}$$

In the second equality of Eq. (1a), $\mathcal{T}\mathcal{H}\mathcal{T}^{-1}$ represents the effect of time reversal on \mathcal{H} , which amounts to taking the conjugate of \mathcal{H} (i.e., replacing its ji 's by $-j$'s), while in the third equality of Eq. (1a), $\mathcal{P}\mathcal{H}^*\mathcal{P}$ represents the effect of space reversal on \mathcal{H}^* , where \mathcal{P} is the (spatial) exchange operator [0, 1; 1, 0] [17].

\mathcal{PT} -symmetric systems exhibit a pair of complex eigenfrequencies, $\xi_{1,2} = \omega_{1,2} + j\zeta_{1,2}$, as illustrated in Fig. 3(b) [17]. These eigenfrequencies correspond to two double-sheet Riemann surfaces, as will be shown in the next section. Assuming the time harmonic dependence $\exp(j\xi t)$, ζ_1 and ζ_2 correspond to loss and gain, respectively. These values merge to the value zero at the junction of the two pitchforks, at a specific point of the coupling parameter space, κ_t . This point corresponds to an exact balance between gain and loss in the system, and is called *Exceptional Point* (EP).

A \mathcal{PT} -symmetric system may also be purely passive. This occurs when the imaginary part of the eigenspectrum in Fig. 3(b) is shifted upwards, transforming the negative (gain) ζ_2 into a purely positive (loss) value, while the real part of the eigenspectrum remains unchanged, as shown in Fig. 3(c). Mathematically, this shift corresponds to a *gauge transformation*, which will be explained in the following section.

IV. TIME ANALYSIS (RESONATOR PROBLEM)

A priori, a P-LWA (Fig. 1) seems quite different from a \mathcal{PT} -symmetry system (Fig. 3(a)). However, it is closely related to such a system because its unit cell also supports two coupled resonant modes, or eigenmodes, and consequently also exhibits a complex eigenspectrum of the type shown in Fig. 3(b) or Fig. 3(c). In order to apply \mathcal{PT} -symmetry theory, we first consider, in this section, the *temporal frequency* domain, where the unit cell is excited as a resonator and exhibits therefore complex eigenfrequencies. This domain is the space where one may apply periodic boundary conditions along the (irreducible) Brillouin zone to compute the dispersion diagram of the structure [24]. However, the following analysis will focus on the Γ spectral point, i.e., $\Phi = \beta p = 0$, where Φ is the phase shift across the unit cell, β is the wavenumber and p is the period of the structure; this point, which also implies $\beta = 0$, corresponds to the broadside radiation regime [24].

The two P-LWA modes are shown in Fig. 4.³ One of them, depicted in Fig. 4(a), is a symmetric or *even* mode that is obtained by terminating the unit cell at its two ends with a Perfect Magnetic Conductor (PMC) wall or, equivalently, an open circuit. The other mode, depicted in Fig. 4(b), is an anti-symmetric or *odd* mode that is obtained by terminating the unit cell at its two ends with a Perfect Electric Conductor (PEC) wall or, equivalently, a short circuit. The two eigenmodes in Fig. 4 may be written as^{4,5}

$$\psi_{t,e} = \exp(j\xi_e t) f_e(z) \tag{2a}$$

and

$$\psi_{t,o} = \exp(j\xi_o t) f_o(z), \tag{2b}$$

where the temporal and spatial dependencies have been assumed to be independent of each other, with $f_e(z)$ and $f_o(z)$ being even and odd functions of space along the direction of the antenna axis (z direction), and where

$$\xi_e = \omega_e + j\zeta_e, \tag{3a}$$

and

$$\xi_o = \omega_o + j\zeta_o, \tag{3b}$$

³In contrast to the two-box system in Fig. 3(a), the P-LWA has eigenmode that are essentially *collocated*, i.e., present at the same location of space, but this does not pose any problem as long as their coupling can also be modeled by a coupling coefficient, as will be the case here.

⁴The t subscript in the following expressions emphasizes the related quantities pertain to the domain of temporal complex frequencies, or resonator regime.

⁵We omit here the transverse variables, x and y , as the related dependencies do not play a role in the analysis. Accordingly, the functions ψ represent the part of the (electric or magnetic) field that depends only on the spatial variable z .

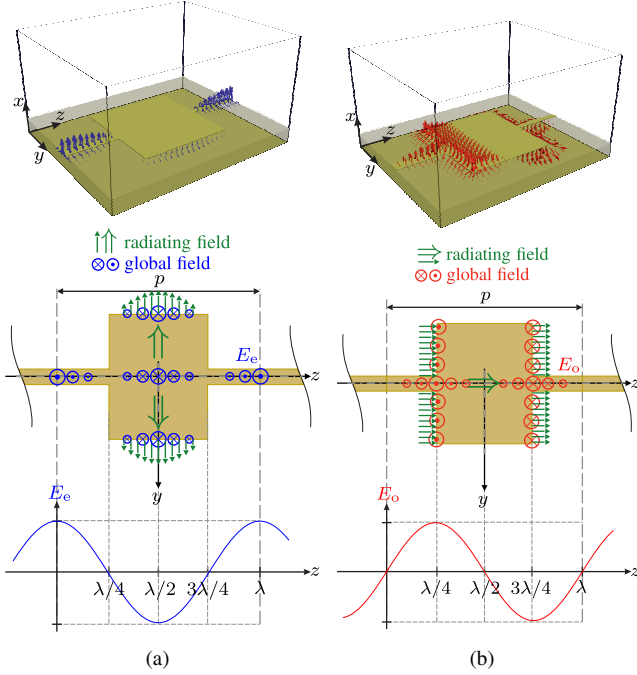


Fig. 4. Complex eigenmodes for the SFP-P-LWA in Fig. 1 or Fig. 2. (a) Even (or symmetric) eigenmode, $\psi_{t,e}$, with eigenfrequency $\xi_e = \omega_e + j\zeta_e$. (b) Odd (or asymmetric) eigenmode, $\psi_{t,o}$, with eigenfrequency $\xi_o = \omega_o + j\zeta_o$.

are the even and odd complex frequencies, where the real parts, ω_e and ω_o , represent the resonators' oscillation frequencies, while the imaginary parts, ζ_e and ζ_o , represent the related power decay once the source has been removed.

In the absence of coupling between the even and odd modes, the P-LWA eigenstates are described by the uncoupled equations

$$\frac{d\psi_{t,e}}{dt} = j\xi_e\psi_{t,e}, \quad (4a)$$

$$\frac{d\psi_{t,o}}{dt} = j\xi_o\psi_{t,o}, \quad (4b)$$

which directly follow from the ansätze in Eq. (2). In contrast, in the presence of coupling, the governing equations of the system become the coupled-mode equations

$$\frac{d\psi_{t,1}}{dt} = j\xi_e\psi_{t,1} + j\kappa_{t,eo}\psi_{t,2}, \quad (5a)$$

$$\frac{d\psi_{t,2}}{dt} = j\kappa_{t,oe}\psi_{t,1} + j\xi_o\psi_{t,2}, \quad (5b)$$

where $\psi_{t,1}$ and $\psi_{t,2}$ are the new modes resulting from the coupling of the even and odd modes, which may be written

$$\psi_{t,1,2}(t) = \exp(j\xi_{1,2}t), \quad (6a)$$

with

$$\xi_{1,2} = \omega_{1,2} + j\zeta_{1,2}, \quad (6b)$$

and where $\kappa_{t,oe}$ and $\kappa_{t,eo}$ are the coupling coefficients from the even mode to the odd mode and vice-versa, which are related as

$$\kappa_{t,eo} = \kappa_{t,oe}^* = \kappa_t, \quad (7)$$

by reciprocity [25].⁶

The complex coupled eigenfrequencies may then be obtained by substituting Eq. (6a) and Eqs. (7) into Eq. (5). This results in the eigenvalue system

$$\begin{bmatrix} \xi_e & \kappa_t \\ \kappa_t^* & \xi_o \end{bmatrix} \begin{bmatrix} \psi_{t,1} \\ \psi_{t,2} \end{bmatrix} = \xi \begin{bmatrix} \psi_{t,1} \\ \psi_{t,2} \end{bmatrix}, \quad (8a)$$

whose eigenvalues are found to be

$$\xi_{1,2} = \frac{\xi_o + \xi_e}{2} \pm \sqrt{\kappa_t^2 + \left(\frac{\xi_o - \xi_e}{2}\right)^2}. \quad (8b)$$

As expected, the system obtained in Eqs. (8) corresponds to the system described in Sec. III [17] and is, hence, \mathcal{PT} -symmetric; the formal proof is given in Appendix A, where the loss-loss eigensystem (8) is first transformed into a gain-loss system by a gauge transformation (Appendix A.I) and where this new system is then shown to satisfy the condition (1) (Appendix A.II). The eigenfrequencies in Eq. (8b) may be separated in terms of real and imaginary parts, which, from Eq. (6b), correspond to the functions $\omega_{1,2}$ and $\zeta_{1,2}$, of κ_t , ω_e , ω_o , ζ_e and ζ_o , each of which is a two-sheet Riemann surface with the upper and lower sheets corresponding to the positive and negative signs in the equations. The two surfaces are plotted versus $\omega_o - \omega_e$ and κ_t in Fig. 5 for the SFP structure in Fig. 1.

Under the *frequency balancing* condition,

$$\omega_o = \omega_e = \omega_0, \quad (9)$$

which is known as a necessary condition to avoid a gap that would otherwise separate the backward and forward regimes of P-LWA radiation [24], Eq. (8b) reduces to

$$\xi_{1,2} = \omega_0 + j\zeta_\Sigma \pm \sqrt{\kappa_t^2 - \zeta_\Delta^2}, \quad (10)$$

where

$$\zeta_\Sigma = (\zeta_e + \zeta_o)/2, \quad (11a)$$

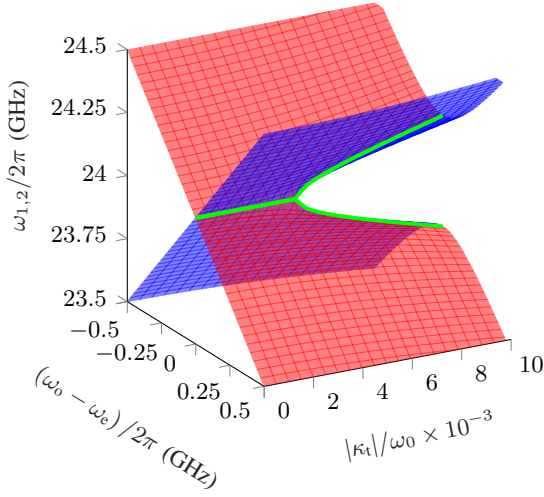
$$\zeta_\Delta = (\zeta_e - \zeta_o)/2. \quad (11b)$$

This corresponds to the cut planes $\omega_o - \omega_e = 0$ that are highlighted by the green curves in Fig. 5.⁷ These curves qualitatively correspond to the pitchfork spectrum in Fig. 3(c) and are therefore associated with the EP shown in Fig. 3(b) or Fig. 3(c). That point is in fact the branch point of the Riemann surface. It is found by eliminating the radicand in (10). This leads to the coupling coefficient

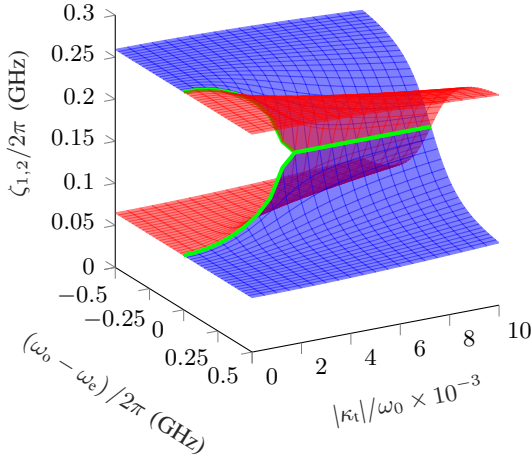
$$\kappa_{t,EP} = \zeta_\Delta = \frac{\zeta_e - \zeta_o}{2}, \quad (12)$$

⁶Specifically, this equality is justified as follows. The factors $\kappa_{t,eo}$ and $\kappa_{t,oe}$ represent exchanges of energy in opposite directions between the eigenmodes, and changing direction corresponds to time reversal or, equivalently, phase conjugation; so, $\kappa_{t,oe}^*$ corresponds to a reversal of exchange direction with respect to $\kappa_{t,eo}$. Moreover, the system has no external force (biasing field or modulation); therefore, the system must be time-reversal symmetric. Thus, one must have $\kappa_{t,eo} = \kappa_{t,oe}^*$.

⁷The whole system governed by Eqs. (8) is called \mathcal{PT} -symmetric by abuse of language. In reality, only the “ \mathcal{PT} -tuned” [26] pitchfork curves corresponding to $\omega_o = \omega_e$ and highlighted in green in the figure are \mathcal{PT} -symmetric according to the definition in Eq. (1), as shown in Appendix A.II.



(a)



(b)

Fig. 5. Riemann surfaces corresponding to the complex coupled temporal eigenfrequencies in Eq. (8b) versus $(\omega_0 - \omega_e)/2\pi$ and κ_t/ω_0 with $\xi_e/2\pi = (24 + j0.028)$ GHz and $\xi_o/2\pi = (24 + j0.287)$ GHz for the SFP-P-LWA in Fig. 1.

whose insertion into Eq. (10) reduces the eigenfrequency to

$$\xi_{EP} = \omega_0 + j\zeta_\Sigma. \quad (13)$$

Let us finally determine the coupled quality factors at the EP. The quality factor is generally defined as

$$Q_{1,2} = \frac{\omega_{t,1,2}}{2\zeta_{t,1,2}}. \quad (14)$$

Inserting Eq. (13) into this relation yields

$$Q_{EP} = Q_1 = Q_2 = \frac{\omega_0}{2\zeta_\Sigma} = \frac{\omega_0}{\zeta_e + \zeta_o} = \frac{2}{\frac{1}{Q_o} + \frac{1}{Q_e}}. \quad (15)$$

That is exactly the *Q-balancing* condition that was found in [14], via circuit modeling, to be the second condition for solving the broadside issue!

Figure 6 presents two-dimensional graphs for the complex eigenfrequencies (2D version of Fig. 5 in the plane

$(\omega_o - \omega_e) = 0$ and for the quality factors using the temporal parameters in Tab. I. The complex eigenfrequencies [Eq. (10)], plotted in Fig. 6(a), exhibit exactly the loss-loss pitchfork spectrum in Fig. 3(c),⁸ with the EP at the junctions of the two pitchforks, while the *Q*-factors [Eq. (14)], plotted in Fig. 6(b) merge at the EP.

TABLE I
TEMPORAL FREQUENCY PARAMETERS (IN GHz) OBTAINED BY FULL-WAVE SIMULATION FOR THE SFP P-LWA IN FIG. 1.

$\omega_0/2\pi$	$\xi_e/2\pi$	$\xi_o/2\pi$	$\zeta_\Sigma/2\pi$	$\zeta_\Delta/2\pi$
24	$24 + j0.028$	$24 + j0.287$	0.1575	-0.1295

In summary, we have demonstrated in this section, using coupled-mode theory, that a P-LWA is a *PT*-symmetric system with an EP and that this exceptional point corresponds to the satisfaction of the twofold *frequency balancing and Q-balancing condition* found by a circuit approach in previous research as being the solution to the broadside issue [12]–[14]. This is comforting, but not sufficient: our intention here is to establish a theory that is self-consistent.

V. TIME TO SPACE MAPPING

The temporal-frequency analysis performed in the previous section revealed that a P-LWA is a *PT*-symmetric system and identified its EP. However, the related resonator or standing-wave regime does *not* correspond to the operation regime of the antenna, which functions as a propagation or traveling-wave system. Therefore, we need to perform a temporal-frequency to spatial-frequency mapping in order to gain information on the physics of the EP and find out whether it indeed corresponds to the resolution of the broadside issue, as suggested from comparison with [12]–[14] in the previous section.

Such a mapping from temporal frequencies, $\xi = \omega + j\zeta$, to spatial frequencies, $\gamma = \alpha + j\beta$, has been a subject of investigation for over a decade [27]–[30]. This research culminated in a theory and procedure presented in [30], which leverages analytical continuity for mapping the ξ and ζ complex planes to each other for arbitrary problems. The procedure is particularly simple when the solution of the system is available in analytical form in the starting plane, as is the case in our P-LWA analysis, in which case it reduces to the following two steps:

- 1) replace the (complex) frequency variable ξ by the (real) frequency variable ω ;
- 2) replace the (real) variable $\beta(\xi)$ by $-j\gamma(\omega)$;
- 3) solve the resulting equation for γ .

The mapping procedure must be applied here to the complex temporal frequency ξ . However, the currently available formula, given by Eq. (10), is not a function of β . This is because it has been derived for the Γ point of the reciprocal space, $\Phi = \beta p = 0$, corresponding to the broadside point of the P-LWA. Moving now to the complex spatial frequency

⁸There is in fact a small difference: the slight divergence of ζ_1 and ζ_2 form ζ_Σ for increasing κ_s in the broken *PT*-symmetry region (right of the EP). This divergence is due to small detuning from ω_0 as the level of asymmetry increases and is nonessential here insofar as it does not concern the EP.

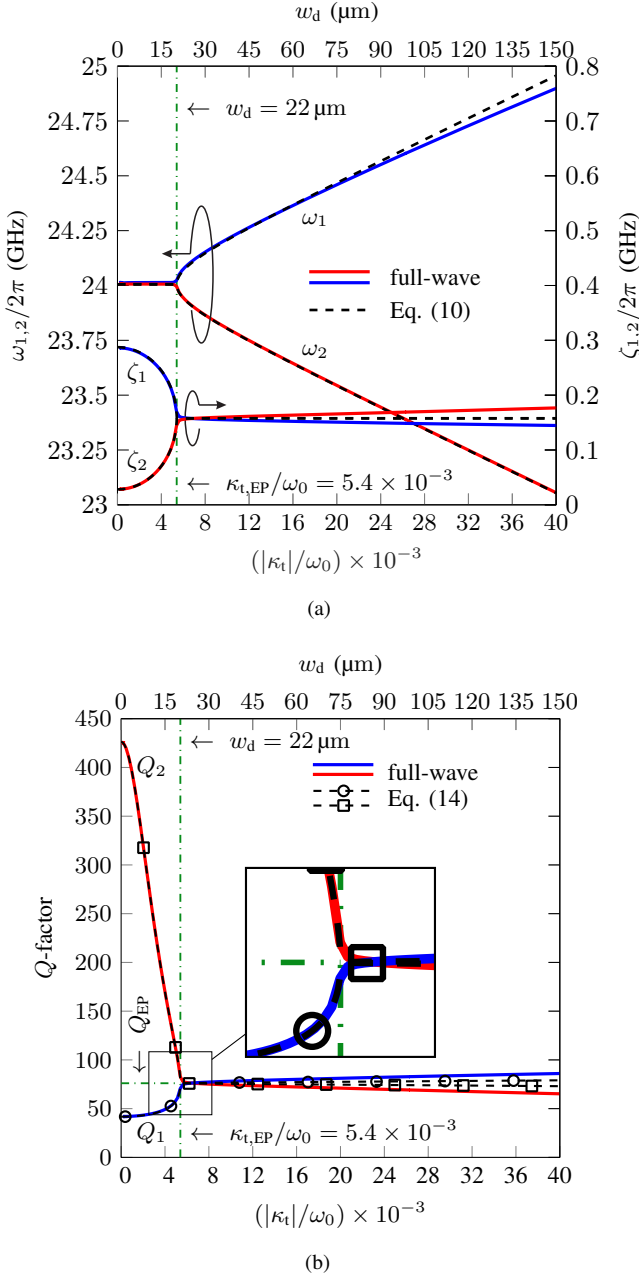


Fig. 6. Analytical and full-wave (CST) results for the SFP P-LWA in Fig. 1. (a) Coupled complex eigenfrequencies [Eq. (10)]. (b) Coupled Q -factors [Eq. (14)].

($\gamma = \alpha + j\beta$) plane to investigate the frequency scanning operation of the P-LWA naturally requires introducing the β variable in Eq. (10). This can be done at this point by realizing that $\Phi = \beta p \neq 0$ must act a contribution to coupling, viz., as part of κ_t (in rad/s) in Eqs. (5), so that the total coupling coefficient decomposes as

$$\kappa_t = \sqrt{\left(\frac{\omega_0 \Phi}{2\pi}\right)^2 + \kappa_{t,\text{ga}}^2} = \sqrt{\left(\frac{\omega_0 \beta p}{2\pi}\right)^2 + \kappa_{t,\text{ga}}^2}, \quad (16)$$

where $\kappa_{t,\text{ga}}$ is the coupling coefficient due to geometrical asymmetry [Fig. 2], while $\omega_0 \Phi / 2\pi = \omega_0 \beta p / 2\pi$ appears to be a contribution to the overall coupling that is due to propagation

phase shifting across a unit cell. Note that this contribution disappears at broadside, where only geometrical asymmetry remains as the expected remedy to the broadside issue.

Substituting Eq. (16) into Eq. (10), we get

$$\xi_{1,2} = \omega_0 + j\zeta_\Sigma \pm \sqrt{\left(\frac{\omega_0 \beta p}{2\pi}\right)^2 + \kappa_{t,\text{ga}}^2 - \zeta_\Delta^2}, \quad (17)$$

which, including now β , is an adequate formula for mapping. So, we proceed to the mapping procedure. First, we substitute $\xi_{1,2}$ by ω and β by $-j\gamma$, and then we solve the resulting equation for γp , which yields

$$\gamma_{1,2} p = \pm \frac{j2\pi}{\omega_0} \sqrt{(\omega - \omega_0 - j\zeta_\Sigma)^2 + \zeta_\Delta^2 - \kappa_{t,\text{ga}}^2}. \quad (18)$$

Interestingly, inserting the EP coupling factor at broadside, i.e., Eq. (12) with $\kappa_{t,\text{ga}} = \kappa_{t,\text{EP}}$ into Eq. (18) reduces the dispersion relation to

$$\gamma_{1,2;\text{EP}} p = \pm \frac{j2\pi}{\omega_0} \sqrt{(\omega - \omega_0 - j\zeta_\Sigma)^2}, \quad (19a)$$

or

$$\gamma_{1,2;\text{EP}} p = (\alpha + j\beta)p = \pm \frac{j2\pi}{\omega_0} (\omega - \omega_0 - j\zeta_\Sigma), \quad (19b)$$

so that

$$\beta_{\text{EP}} p = \pm 2\pi \frac{\omega - \omega_0}{\omega_0}, \quad (20a)$$

which retrieves the expected result $\beta(\omega = \omega_0) = 0$, and

$$\alpha_{\text{EP}} p = \pm 2\pi \frac{\zeta_\Sigma}{\omega_0}, \quad (20b)$$

which is frequency-independent. The frequency independence of α , or flat $\alpha(\omega)$ curve, is a known condition for smooth transition across broadside [11], [14]. However, this is still not a sufficient condition: given the asymmetry of the P-LWA structure [see Fig. 2(b)], which will be discussed in the next section, the antenna must exhibit different impedances at its two ports, and therefore the two ports cannot be matched to a single external impedance, R_0 . So, the additional impedance matching condition will be satisfied at best at only one of the two ports.

Figure 7 compares the theoretical⁹ and full-wave simulated complex spatial eigenfrequency, $\gamma = \alpha + j\beta$. Figure 7(a) shows the manifestation of the broadside issue for a symmetrical P-LWA ($\kappa_t = 0$) in terms of the deviation of α from a straight line, while Fig. 7(b) shows the spatial spectrum of a P-LWA with optimal asymmetry in terms of a frequency-independent α , consistent with Eq. (20a).

⁹Remarkably, the theoretical curves in the figure can be plotted analytically, using Eq. (18), on the basis of a single full-wave eigenfrequency simulation, specifically the simulation of the initial, symmetric version of the P-LWA structure, which provides the even and odd eigenfrequencies. Indeed, the parameters ω_0 and $\zeta_{\Sigma,\Delta}$ depend solely on $\omega_{e,o}$ and $\zeta_{e,o}$, according to Eqs. (9) and (11), respectively, while $\kappa_{t,\text{ga}}$ is zero in the symmetric case and also depending only on $\zeta_{e,o}$ at the EP, according to Eq. (12).

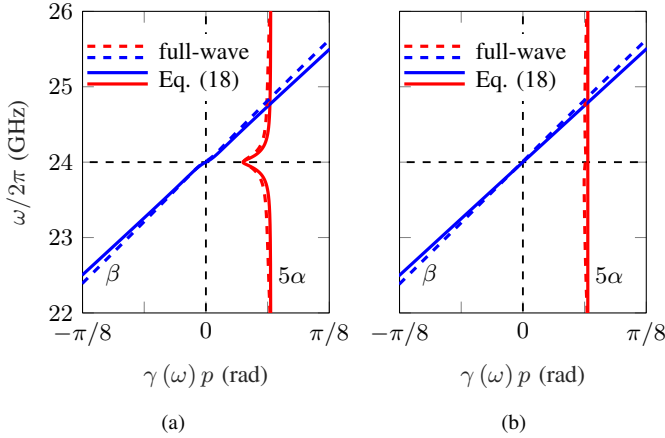


Fig. 7. Full-wave and analytically mapped complex spatial eigenfrequencies [Eq. (18)] for the SFP LWA in Fig. 1. (a) Symmetrical SFP LWA with $\kappa = 0$ or $w_d = 0$. (b) Asymmetrical SFP LWA with $\kappa_t = \kappa_{t,EP}$ or $w_d = 22 \mu\text{m}$ (see Fig. 6).

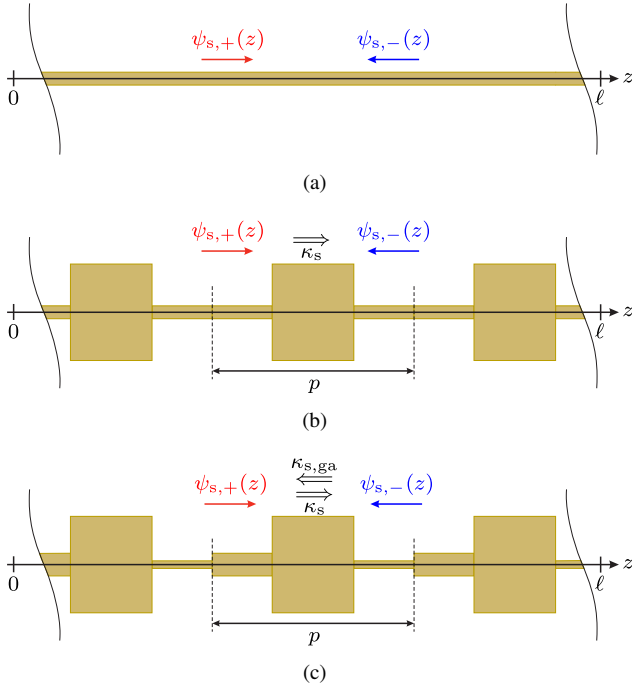


Fig. 8. Three successive steps to determine the impedance of a P-LWA at its two ends. (a) Uniform transmission line. (b) Periodically loaded transmission line with symmetric unit cell. (c) Same as (b) but with an asymmetric unit cell, as in Fig. 2(b).

VI. SPACE ANALYSIS (WAVEGUIDE PROBLEM)

We shall derive here formulas for the impedances at the two ends of an asymmetric P-LWA [see Fig. 2(b)] in the three successive and progressive steps indicated in Fig. 8, in order to find out whether the EP complex spatial frequency in Eq. (19) indeed corresponds to the resolution of the broadside issue at one of the two ends of the structure.

Let us start with a uniform transmission line, shown

in Fig. 8(a), which we assume to be dispersionless¹⁰ and matched. Such a structure admits *forward and backward waves*, with complex wavenumbers $+\gamma_0$ and $-\gamma_0$, respectively. The corresponding waveforms are¹¹

$$\psi_{s;\pm}(t, z) = e^{j\omega t} e^{\mp\gamma_0 z}, \quad (21a)$$

where

$$\gamma_0 = \alpha + j\beta. \quad (21b)$$

Given the uniformity of the transmission line and matching assumption, these waves are not coupled and satisfy then the uncoupled equations

$$\frac{d\psi_{s,+}}{dz} = -\gamma_0 \psi_{s,+}, \quad (22a)$$

$$\frac{d\psi_{s,-}}{dz} = \gamma_0 \psi_{s,-}, \quad (22b)$$

which are the spatial counterparts of Eqs. (4).

Let us move on to the symmetric periodic structure in Fig. 8(b), which represents the P-LWA category in Fig. 2(a). Now the forward and backward waves are coupled by periodic scattering along the structure and become therefore an infinite set of *forward and backward space harmonics*. Consequently, Eqs. (22) are augmented to the coupled equations [31],

$$\frac{d\psi_{s,1}}{dz} = -\gamma_0 \psi_{s,1} - j\kappa_s \exp\left(-j\frac{4\pi}{p}z\right) \psi_{s,2}, \quad (23a)$$

$$\frac{d\psi_{s,2}}{dz} = j\kappa_s^* \exp\left(-j\frac{4\pi}{p}z\right) \psi_{s,1} + \gamma_0 \psi_{s,2}, \quad (23b)$$

where the coupling terms include the periodicity of the structure, consistent with the fact that coupling is periodic. In order to access the eigenvalues, we may apply the transformation [31]

$$\begin{bmatrix} \psi_{s,1} \\ \psi_{s,2} \end{bmatrix} = j \begin{bmatrix} \exp(-j2\pi/pz) & 0 \\ 0 & \exp(j2\pi/pz) \end{bmatrix} \begin{bmatrix} \Psi_{s,1} \\ \Psi_{s,2} \end{bmatrix} \quad (24)$$

to Eqs. (23), which allows us to factor out the term $\exp(j4\pi/pz)$ and leads to the new coupled system

$$\frac{d}{dz} \begin{bmatrix} \Psi_{s,1} \\ \Psi_{s,2} \end{bmatrix} = \begin{bmatrix} -\gamma_{0,p} & -j\kappa_s \\ j\kappa_s^* & \gamma_{0,p} \end{bmatrix} \begin{bmatrix} \Psi_{s,1} \\ \Psi_{s,2} \end{bmatrix}, \quad (25a)$$

where

$$\gamma_{0,p} = \alpha + j\left(\beta - \frac{2\pi}{p}\right), \quad (25b)$$

and whose eigensolutions are found to be

$$\gamma_{1,2}(\omega) = \pm \sqrt{\gamma_{0,p}^2 - |\kappa_s|^2}. \quad (26)$$

Let us finally consider the asymmetric periodic structure in Fig. 8(c), which represents the P-LWA category in Fig. 2(b). The related coupled equations are formally identical to those of Eqs. (25), except for an additional coupling term accounting

¹⁰The microwave transmission lines that constitute the backbone of typical P-LWAs, such as microstrip and coplanar transmission lines, are indeed essentially dispersionless in the frequency range of interest.

¹¹The s subscript in the following expressions emphasizes the related quantities pertains to the domain of spatial complex frequencies, or waveguide regime.

for coupling due to the geometrical asymmetry, $\kappa_{s,ga}$. Thus, the coupled mode system reads

$$\frac{d}{dz} \begin{bmatrix} \Psi_{s,1} \\ \Psi_{s,2} \end{bmatrix} = \begin{bmatrix} -\gamma_{0,p} & -j(\kappa_s + j\kappa_{s,ga}) \\ j(\kappa_s^* - j\kappa_{s,ga}^*) & \gamma_{0,p} \end{bmatrix} \begin{bmatrix} \Psi_{s,1} \\ \Psi_{s,2} \end{bmatrix} \quad (27)$$

and the related eigenvalues are found to be

$$\gamma_{1,2}(\omega) = \pm \sqrt{\gamma_{0,p}^2 - |\kappa_s|^2 + |\kappa_{s,ga}|^2}. \quad (28)$$

Comparing the temporal [Eq. (18)] and spatial frequencies [Eq. (28)] yields

$$\begin{aligned} \gamma_{0,p}^2 - |\kappa_s|^2 + |\kappa_{s,ga}|^2 \\ = - \left(\frac{2\pi}{\omega_0 p} \right)^2 \left[(\omega - \omega_0 - j\zeta_\Sigma)^2 + \zeta_\Delta^2 - \kappa_{t,ga}^2 \right], \end{aligned} \quad (29a)$$

or

$$\gamma_{0,p} = j2\pi \frac{\omega - \omega_0 - j\zeta_\Sigma}{\omega_0 p}, \quad (29b)$$

$$|\kappa_s| = \frac{2\pi\zeta_\Delta}{\omega_0 p}, \quad (29c)$$

$$|\kappa_{s,ga}| = \frac{2\pi\kappa_{t,ga}}{\omega_0 p}, \quad (29d)$$

and hence

$$|\kappa_{s,EP}| = \frac{2\pi\kappa_{t,EP}}{\omega_0 p}. \quad (29e)$$

These relations are useful because they directly provide the spatial quantities in Sec. VI from the temporal quantities in Sec. IV without requiring the space to time mapping in Sec. V.

We may now derive the sought-after impedance formulas for the asymmetric P-LWA. The waves at the two ends of the structure, assumed to be of length ℓ ,¹² are related by the transfer matrix $\exp(jM_s\ell)$ as [31]

$$\begin{bmatrix} \Psi_{s,1}(0) \\ \Psi_{s,2}(0) \end{bmatrix} = \exp(jM_s\ell) \begin{bmatrix} \Psi_{s,1}(\ell) \\ \Psi_{s,2}(\ell) \end{bmatrix}, \quad (30a)$$

where

$$M_s = \begin{bmatrix} -\gamma_{0,p} & -j(\kappa_s + \kappa_{s,ga}) \\ j(\kappa_s - \kappa_{s,ga}) & \gamma_{0,p} \end{bmatrix}, \quad (30b)$$

with $(\kappa_s - \kappa_{s,ga})^* = (\kappa_s - \kappa_{s,ga})$ from reciprocity, and

$$\begin{aligned} \exp(jM_s\ell) &= \begin{bmatrix} U_{11} & U_{12} \\ U_{21} & U_{22} \end{bmatrix} = \\ &= \begin{bmatrix} \cosh(\gamma\ell) + j\frac{\gamma_{0,p}}{\gamma} \sinh(\gamma\ell) & j\frac{(\kappa_s + \kappa_{s,ga})}{\gamma} \sinh(\gamma\ell) \\ -j\frac{(\kappa_s - \kappa_{s,ga})}{\gamma} \sinh(\gamma\ell) & \cosh(\gamma\ell) - j\frac{\gamma_{0,p}}{\gamma} \sinh(\gamma\ell) \end{bmatrix}, \end{aligned} \quad (30c)$$

where γ was defined by Eq. (28). Rearranging the previous system in terms of scattering parameters yields

$$\begin{bmatrix} \Psi_{s,2}(0) \\ \Psi_{s,1}(\ell) \end{bmatrix} = \begin{bmatrix} \Gamma_+ & T \\ T & \Gamma_- \end{bmatrix} \begin{bmatrix} \Psi_{s,1}(0) \\ \Psi_{s,2}(\ell) \end{bmatrix}, \quad (31a)$$

¹²The total length of a periodic structure is Np , where N is the total number of unit cells.

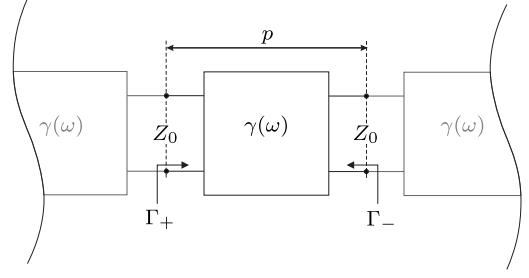


Fig. 9. Equivalent two-port network model for the calculation of the forward and backward Bloch impedances, Z_B^\pm , in Eq. (33) with Z_0 being the homogenized reference impedance.

from which we obtain the forward reflection coefficient

$$\Gamma_+ = \frac{U_{21}}{U_{11}} = - \frac{j \frac{(\kappa_s - \kappa_{s,ga})}{\gamma} \sinh(\gamma\ell)}{\cosh(\gamma\ell) + j \frac{\gamma_{0,p}}{\gamma} \sinh(\gamma\ell)}, \quad (32a)$$

the backward reflection coefficient

$$\Gamma_- = - \frac{U_{12}}{U_{22}} = - \frac{j \frac{(\kappa_s + \kappa_{s,ga})}{\gamma} \sinh(\gamma\ell)}{\cosh(\gamma\ell) - j \frac{\gamma_{0,p}}{\gamma} \sinh(\gamma\ell)}, \quad (32b)$$

and the transmission coefficient

$$T = \frac{1}{U_{11}} = \frac{1}{\cosh(\gamma\ell) + j \frac{\gamma_{0,p}}{\gamma} \sinh(\gamma\ell)}. \quad (32c)$$

Moreover, the Bloch impedance in the forward and backward directions, Z_B^\pm , can be calculated after transforming the scattering matrix [Eq. (30c)] into the ABCD-matrix, as [32]

$$\frac{Z_B^\pm}{Z_0} = \frac{-2B}{A - D \mp \sqrt{(A + D)^2 - 4}}, \quad (33)$$

where Z_0 is the reference impedance¹³ for a two-port network model, as shown in Fig. 9.

Figure 10 plots the spatial eigenfrequency γ and the normalized Bloch impedances Z_B^\pm/Z_0 for the spatial parameters listed in Tab. II. In the symmetric case ($\kappa_s = 0$), corresponding to Fig. 10(a), the forward and backward impedances¹⁴ are, as expected, identical and peaking at $\omega_0/2\pi = 24$ GHz. Meanwhile, the leakage factor (α) shows a dip and the propagation constant (β) exhibits slight nonlinearity at ω_0 , both indicating a Q -mismatch. In contrast, in the EP-asymmetric case ($\kappa_{s,ga} = \kappa_{s,EP}$) [Fig. 10(b)], the forward and backward Bloch impedances are different, as expected from the unequal forward and backward reflection coefficients ($\Gamma_+ \neq \Gamma_-$) [Eq. (32)]. While Z_B^- is highly dispersive, Z_B^+ is *frequency-independent*, consistently with

$$\Gamma_+(\kappa_{s,ga} = \kappa_{s,EP}) = 0, \quad (34)$$

¹³The reference impedance Z_0 for the simple transmission line in Fig. 8(a) is the characteristic impedance, whereas for the periodic structures in Figs. 8(b) and 8(c), Z_0 depends on the impedance step and the reference location.

¹⁴The negative sign in the backward impedance is simply due to the oppositely flowing ($-z$) current in the fixed coordinate system.

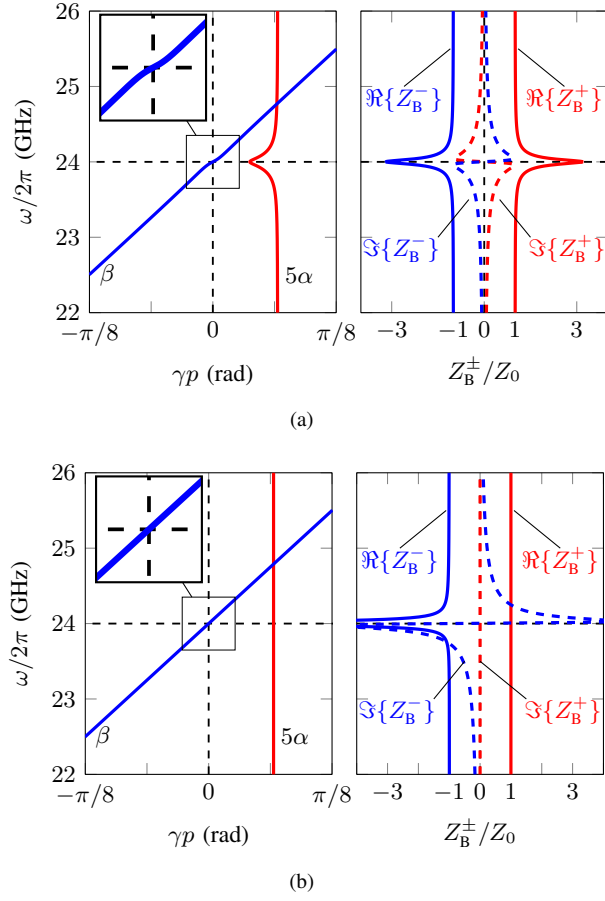


Fig. 10. Analytical results for the spatial eigenfrequency [Eq. (28)], using Tab. II] and Bloch impedance [Eq. (33)]. (a) Symmetric structure with $\kappa_s = 0$ [Fig. 8(b)] and (b) asymmetric structure at EP with $\kappa_{s,ga} = \kappa_{s,EP} = \zeta_{\Delta}/\omega_0 p$ [Fig. 8(c)].

which reveals that the P-LWA is matched in the forward direction. Moreover, the leakage factor and propagation constant are perfectly flat and linear, respectively, confirming the expected resolution of the broadside issue, for the source placed at one of the two ends of the structure. This completes our \mathcal{PT} -symmetry-based demonstration that a frequency-balanced and Q -balanced P-LWA provides seamless scanning through broadside if fed at its “good” input.

TABLE II
SPATIAL PARAMETERS OBTAINED FROM THE TEMPORAL PARAMETERS IN TAB. I USING EQS. (29). ALL THE UNITS ARE IN RAD/M.

$\gamma_{0,p}(\omega = \omega_0)$	$ \kappa_s $	$ \kappa_{s,EP} $
6.3072	5.1816	5.1816

VII. CONCLUSION

We have presented an electromagnetic theory of seamless-scanning P-LWAs based on the concept of \mathcal{PT} -symmetry. After demonstrating that a P-LWA is a \mathcal{PT} -symmetric system, we have shown that the long-standing issue of gain degradation at broadside is resolved by introducing in the P-LWA’s unit cell an amount of geometrical asymmetry that corresponds to the EP of the \mathcal{PT} -symmetry spectrum.

This theory provides a solid foundation for the twofold condition of frequency balancing and Q -balancing that was discovered using circuit modeling in previous works. Moreover, it represents an original contribution to the field of \mathcal{PT} -symmetry by extending the concept from single-space to double-space, space-time \mathcal{PT} -symmetry.

APPENDIX A APPENDIX: P-LWA \mathcal{PT} -SYMMETRY

The \mathcal{PT} -Symmetry of a P-LWA may be shown in two steps: the transformation of its loss-loss eigenspectrum into a gain-loss eigenspectrum, which will be performed in Sec. A.I, and the \mathcal{PT} -symmetry demonstration of that equivalent gain-loss system, which will be performed in Sec. A.II.

A.I Gauge Transformation from Passive to Active \mathcal{PT} -Symmetry

Inserting Eqs. (3) with balanced frequencies [Eqs. (9): $\omega_e = \omega_o = \omega_0$] and real coupling factor ($\kappa_t^* = \kappa_t$) into Eq. (5) yields the Schrödinger equation

$$-j \frac{d}{dt} \begin{bmatrix} \psi_{t,1} \\ \psi_{t,2} \end{bmatrix} = \mathcal{H} \begin{bmatrix} \psi_{t,1} \\ \psi_{t,2} \end{bmatrix}, \quad (35a)$$

with the Hamiltonian

$$\mathcal{H} = \begin{bmatrix} \omega_0 + j\zeta_e & \kappa_t \\ \kappa_t & \omega_0 + j\zeta_o \end{bmatrix}. \quad (35b)$$

Then, inserting the gauge transformation [17]

$$\begin{bmatrix} \psi_{t,1} \\ \psi_{t,2} \end{bmatrix} = \exp(\zeta_{\Sigma} t) \begin{bmatrix} \psi'_{t,1} \\ \psi'_{t,2} \end{bmatrix}, \quad (36)$$

where $\psi'_{t,1}$ and $\psi'_{t,2}$ are the gauge-transformed fields and ζ_{Σ} is given by Eq. (11a), into Eq. (35a), we get

$$\begin{aligned} j \frac{d}{dt} \begin{bmatrix} \psi'_{t,1} \\ \psi'_{t,2} \end{bmatrix} &= \begin{bmatrix} \omega_0 + j\zeta_e & \kappa_t \\ \kappa_t & \omega_0 + j\zeta_o \end{bmatrix} \begin{bmatrix} \psi'_{t,1} \\ \psi'_{t,2} \end{bmatrix} - j\zeta_{\Sigma} \begin{bmatrix} \psi'_{t,1} \\ \psi'_{t,2} \end{bmatrix} \\ &= \begin{bmatrix} \omega_0 + j\zeta_{\Delta} & \kappa_t \\ \kappa_t & \omega_0 - j\zeta_{\Delta} \end{bmatrix} \begin{bmatrix} \psi'_{t,1} \\ \psi'_{t,2} \end{bmatrix}, \end{aligned} \quad (37)$$

where ζ_{Σ} is given by Eq. (11b). The matrix

$$\mathcal{H}' = \begin{bmatrix} \omega_0 + j\zeta_{\Delta} & \kappa_t \\ \kappa_t & \omega_0 - j\zeta_{\Delta} \end{bmatrix} \quad (38)$$

in this relation is the Hamiltonian of the gauge-transformed version of \mathcal{H} in Eq. (35b). While \mathcal{H} represents a \mathcal{PT} -symmetric loss-loss system, recognized by its two positive signs, \mathcal{H}' represents a \mathcal{PT} -symmetric gain-loss system, recognized by its negative and positive signs.

A.II Demonstration of the P-LWA \mathcal{PT} -Symmetry

A P-LWA antenna is governed by the loss-loss Hamiltonian \mathcal{H} in Eq. (35b) or by its gauge-transformed version \mathcal{H}' in Eq. (38). Let consider \mathcal{H}' . According to Eq. (1), and noting

that $\mathcal{P}^* = \mathcal{P}$, a system described by \mathcal{H}' is \mathcal{PT} -symmetric if $\mathcal{P}\mathcal{H}'^*\mathcal{P} = \mathcal{H}'$. Let us test this condition:

$$\begin{aligned} \mathcal{P}\mathcal{H}'^*\mathcal{P} &= \begin{bmatrix} 0 & 1 \\ 1 & 0 \end{bmatrix} \begin{bmatrix} \omega_0 + j\zeta_\Delta & \kappa_t \\ \kappa_t & \omega_0 - j\zeta_\Delta \end{bmatrix}^* \begin{bmatrix} 0 & 1 \\ 1 & 0 \end{bmatrix} \\ &= \begin{bmatrix} 0 & 1 \\ 1 & 0 \end{bmatrix} \begin{bmatrix} \omega_0 - j\zeta_\Delta & \kappa_t \\ \kappa_t & \omega_0 + j\zeta_\Delta \end{bmatrix} \begin{bmatrix} 0 & 1 \\ 1 & 0 \end{bmatrix} \\ &= \begin{bmatrix} \omega_0 + j\zeta_\Delta & \kappa_t \\ \kappa_t & \omega_0 - j\zeta_\Delta \end{bmatrix} = \mathcal{H}'. \end{aligned} \quad (39)$$

The condition is satisfied. So, a frequency-balanced P-LWA is a \mathcal{PT} -symmetric system.

Note that \mathcal{PT} -symmetry occurs *only in the balanced-frequency regime*. Indeed outside of this regime, Eqs. (39) become

$$\begin{aligned} \mathcal{P}\mathcal{H}'^*\mathcal{P} &= \begin{bmatrix} 0 & 1 \\ 1 & 0 \end{bmatrix} \begin{bmatrix} \omega_e + j\zeta_\Delta & \kappa_t \\ \kappa_t & \omega_o - j\zeta_\Delta \end{bmatrix}^* \begin{bmatrix} 0 & 1 \\ 1 & 0 \end{bmatrix} \\ &= \begin{bmatrix} 0 & 1 \\ 1 & 0 \end{bmatrix} \begin{bmatrix} \omega_e - j\zeta_\Delta & \kappa_t \\ \kappa_t & \omega_o + j\zeta_\Delta \end{bmatrix} \begin{bmatrix} 0 & 1 \\ 1 & 0 \end{bmatrix} \\ &= \begin{bmatrix} \omega_o + j\zeta_\Delta & \kappa_t \\ \kappa_t & \omega_e - j\zeta_\Delta \end{bmatrix} \neq \mathcal{H}'. \end{aligned} \quad (40)$$

This fact is also apparent in the Riemann sheets of Fig. 5 and consistent with the well-known necessity of frequency balancing for P-LWA seamless radiation through broadside [24].

REFERENCES

- [1] D. R. Jackson and A. A. Oliner, "Leaky-wave antennas," in *Modern Antenna Handbook*, C. A. Balanis, Ed. Wiley, 2007, chap. 7.
- [2] C. Caloz, D. R. Jackson, and T. Itoh, "Leaky-wave antennas," in *Frontiers in Antennas: Next Generation Design and Engineering*, F. B. Gross, Ed. McGraw Hill, 2011, chap. 9.
- [3] D. R. Jackson, C. Caloz, and T. Itoh, "Leaky-wave antennas," *Proc. IEEE*, vol. 100, no. 7, pp. 2194–2206, Jul. 2012.
- [4] W. Menzel, "A new travelling wave antenna in microstrip," in *8th IEEE European Microw. Conf. (EuMC)*, Paris, France, Oct. 1978.
- [5] S. Abielmona, H. V. Nguyen, and C. Caloz, "Analog direction of arrival estimation using an electronically-scanned CRLH leaky-wave antenna," *IEEE Trans. Antennas Propag.*, vol. 59, no. 4, pp. 1408–1412, Apr. 2011.
- [6] S. Gupta, S. Abielmona, and C. Caloz, "Microwave analog real-time spectrum analyzer (RTSA) based on the spectral–spatial decomposition property of leaky-wave structures," *IEEE Trans. Microw. Theory Techn.*, vol. 57, no. 12, pp. 2989–2999, Dec. 2009.
- [7] K. van Caekenberghe, K. F. Brakora, and K. Sarabandi, "A 94 GHz OFDM frequency scanning radar for autonomous landing guidance," in *IEEE Radar Conf.*, Waltham, MA, USA, Apr. 2007.
- [8] S. Li, C. Li, W. Liu, Z. Sun, S. Lang, Z. Lu, X. Zhang, and G. Fang, "Study of terahertz superresolution imaging scheme with real-time capability based on frequency scanning antenna," *IEEE Trans. Terahertz Sci. Technol.*, vol. 6, no. 3, pp. 451–463, May 2016.
- [9] A. Al-Bassam, D. Heberling, and C. Caloz, "Exceptional point perspective of periodic leaky-wave antennas," in *IEEE AP-S Int. Antennas Propagat. (APS)*, Portland, OR, USA, Jul. 2023, pp. 1275–1276.
- [10] L. O. Goldstone and A. A. Oliner, "Leaky-wave antennas I: Rectangular waveguides," *IRE Trans. Antennas Propag.*, vol. 7, no. 4, pp. 307–319, Oct. 1959.
- [11] S. Paulotto, P. Baccarelli, F. Frezza, and D. R. Jackson, "A novel technique for open-stopband suppression in 1-D periodic printed leaky-wave antennas," *IEEE Trans. Antennas Propag.*, vol. 57, pp. 1894–1906, Jul. 2009.
- [12] S. Otto, A. Rennings, K. Solbach, and C. Caloz, "Transmission line modeling and asymptotic formulas for periodic leaky-wave antennas scanning through broadside," *IEEE Trans. Antennas Propag.*, vol. 59, no. 10, pp. 3695–3709, Oct. 2011.
- [13] S. Otto, Z. Chen, A. Al-Bassam, A. Rennings, K. Solbach, and C. Caloz, "Circular polarization of periodic leaky-wave antennas with axial asymmetry: Theoretical proof and experimental demonstration," *IEEE Trans. Antennas Propag.*, vol. 62, no. 4, pp. 1817–1829, Apr. 2014.
- [14] S. Otto, A. Al-Bassam, A. Rennings, K. Solbach, and C. Caloz, "Transversal asymmetry in periodic leaky-wave antennas for block impedance and radiation efficiency equalization through broadside," *IEEE Trans. Antennas Propag.*, vol. 62, no. 10, pp. 5037–5054, Oct. 2014.
- [15] A. Al-Bassam, S. Otto, D. Heberling, and C. Caloz, "Broadside dual-channel orthogonal-polarization radiation using a double-asymmetric periodic leaky-wave antenna," *IEEE Trans. Antennas Propag.*, vol. 65, no. 6, pp. 2855–2864, Jun. 2017.
- [16] C. M. Bender and S. Boettcher, "Real spectra in non-Hermitian Hamiltonians having \mathcal{PT} symmetry," *Phys. Rev. Lett.*, vol. 80, no. 24, pp. 5243–5246, Jun. 1998.
- [17] C. M. Bender, P. E. Dorey, C. Dunning, A. Fring, D. W. Hook, H. F. Jones, S. Kuzhel, G. Lévai, and R. Tateo, *PT Symmetry: In Quantum and Classical Physics*. World Scientific, Jan. 2019.
- [18] H. Hodaei, M.-A. Miri, M. Heinrich, D. N. Christodoulides, and M. Khajavikhan, "Parity-time-symmetric microring lasers," *Science*, vol. 346, no. 6212, pp. 975–978, Nov. 2014.
- [19] B. Peng, Ş. K. Özdemir, F. Lei, F. Monifi, M. Gianfreda, G. L. Long, S. Fan, F. Nori, C. M. Bender, and L. Yang, "Parity-time-symmetric whispering-gallery microcavities," *Nat. Phys.*, vol. 10, no. 5, pp. 394–398, Apr. 2014.
- [20] S. Zhang, Z. Yong, Y. Zhang, and S. He, "Parity-time symmetry breaking in coupled nanobeam cavities," *Sci. Rep.*, vol. 6, no. 1, Apr. 2016.
- [21] L. Feng, R. El-Ganainy, and L. Ge, "Non-Hermitian photonics based on parity-time symmetry," *Nat. Photonics*, vol. 11, no. 12, pp. 752–762, Nov. 2017.
- [22] Ş. K. Özdemir, S. Rotter, F. Nori, and L. Yang, "Parity-time symmetry and exceptional points in photonics," *Nat. Mater.*, vol. 18, no. 8, pp. 783–798, Aug. 2019.
- [23] S. K. Gupta, Y. Zou, X. Zhu, M. Lu, L. Zhang, X. Liu, and Y. Chen, "Parity-time symmetry in non-Hermitian complex optical media," *Adv. Mater.*, vol. 32, no. 27, Dec. 2019.
- [24] C. Caloz and T. Itoh, *Electromagnetic Metamaterials, Transmission Line Theory and Microwave Applications*. Wiley-IEEE Press, 2006.
- [25] C. Caloz, A. Alù, S. Tretyakov, D. Sounas, K. Achouri, and Z.-L. Deck-Léger, "Electromagnetic nonreciprocity," *Phys. Rev. Appl.*, vol. 10, no. 4, p. 047001, Oct. 2018.
- [26] R. El-Ganainy, K. G. Makris, M. Khajavikhan, Z. H. Musslimani, S. Rotter, and D. N. Christodoulides, "Non-Hermitian physics and PT symmetry," *Nat. Phys.*, vol. 14, no. 1, pp. 11–19, Jan. 2018.
- [27] S. Otto, A. Rennings, K. Solbach, and C. Caloz, "Complex frequency versus complex propagation constant modeling and q -balancing in periodic structures," in *IEEE MTT-S Int. Microw. Symp. Dig.*, Jun. 2012.
- [28] W. Dyab, C. Caloz, and S. Otto, "Interpretation of complex frequencies in propagation problems," in *IEEE Int. Symp. Antennas Propag. (ISAP)*, Hobart, TAS, Australia, Nov. 2015.
- [29] J. G. N. Rahmeier, V. Tiukuvaara, and S. Gupta, "Complex eigenmodes and eigenfrequencies in electromagnetics," *IEEE Trans. Antennas Propag.*, vol. 69, no. 8, pp. 4644–4656, Aug. 2021.
- [30] M. Dehmollaian and C. Caloz, "General mapping between complex spatial and temporal frequencies by analytical continuation," *IEEE Trans. Antennas Propag.*, vol. 69, no. 10, pp. 6531–6545, Oct. 2021.
- [31] S. Orfanidis, *Electromagnetic Waves and Antennas*. Sophocles J. Orfanidis, 2016.
- [32] D. M. Pozar, *Microwave Engineering*, 4th ed. Wiley, 2011.